Cation Intercalation and High Volumetric Capacitance of Two-Dimensional Titanium Carbide

Maria R. Lukatskaya,[1,2] Olha Mashtalir,[1,2]* Chang E. Ren,[1,2]* Yohan Dall'Agnese,[1,2,3,4] Patrick Rozier,[3] Pierre Louis Taberna,[3] Michael Naguib,[1,2] Patrice Simon,[3,4] Michel W. Barsoum,[1] Yury Gogotsi[1,2]†

The intercalation of ions into layered compounds has long been exploited in energy storage devices such as batteries and electrochemical capacitors. However, few host materials are known for ions much larger than lithium. We demonstrate the spontaneous intercalation of cations from aqueous salt solutions between two-dimensional (2D) Ti_3C_2 MXene layers. MXenes combine 2D conductive carbide layers with a hydrophilic, primarily hydroxyl-terminated surface. A variety of cations, including Na^+, K^+, NH_4^+, Mg^{2+}, and Al^{3+}, can also be intercalated electrochemically, offering capacitance in excess of 300 farads per cubic centimeter (much higher than that of porous carbons). This study provides a basis for exploring a large family of 2D carbides and carbonitrides in electrochemical energy storage applications using single- and multivalent ions.

With the increased demand for portable and clean energy, electrochemical capacitors have been attracting attention because of their much greater power density and cyclability relative to Li batteries (*1*, *2*). However, electrical double-layer capacitors (EDLCs), in which the capacity is due to the electrosorption of ions on porous carbon electrodes, have limited energy density (*2*). Pseudo-capacitors, in which the capacity is due to redox reactions, provide higher energy densities but usually suffer from shorter cyclic lifetimes. RuO_2 nanosheets have been used in redox capacitors and have shown impressive capacitance and cyclability, but they are quite expensive to produce (*2*, *3*).

Energy density enhancement of capacitors can be achieved by using hybrid devices, which combine a battery-like redox electrode and a porous carbon electrode (*4*). Another approach is to use materials in which charge storage is due to intercalation of ions between atomic layers because the capacitances—even at high discharge rates—are high. For example, nanocrystalline Nb_2O_5 films with storage capacities of ~130 mAh g^{-1} at rates as high as 10 C (charge/discharge in 6 min) for Li^+ ions in organic electrolytes have been reported. The specific structure of this material can best be described as a crystalline network with two-dimensional (2D) transport paths for ions between atomic layers; thus, even thick electrodes show excellent behavior (*5*). Another example is Mg-buserite electrodes, which exhibit good Na^+ ion intercalation capacitances but have poor electrical conductivities (*6*). Most materials for electrodes that can provide intercalation or surface redox capacitances are poor electronic conductors [e.g., graphene oxide or TiO_2 (*7*)] or are hydrophobic [e.g., graphene (*8*)].

Recently, we reported on a large family of 2D materials that we labeled "MXenes," which combine good electrical conductivities with hydrophilic surfaces. MXenes are 2D materials synthesized by the extraction of the "A" layers from the layered carbides or carbonitrides known as MAX phases. The latter have a general formula of $M_{n+1}AX_n$ (n = 1, 2, 3), where M represents a transition metal; A usually represents a III A or IV A element (such as Al, Ga, Si, or Ge); and X represents C and/or N (*9*). The MXenes Ti_3C_2 (*10*), Ti_2C, Ta_4C_3, TiNbC, and $(V_{0.5}Cr_{0.5})_3C_2$ (*11*), have been fabricated by immersing Al-containing MAX powders in HF solution at room or slightly

elevated temperature (*12*). This synthesis procedure leads to the termination of MXene surfaces by primarily O and/or OH groups with some fluorine present. These terminated MXenes are of the form $M_{n+1}X_nT_x$, where T represents surface termination (O, OH, and/or F) and x is the number of termination groups. We recently showed that $Ti_3C_2T_x$ can be readily and spontaneously intercalated with organic molecules such as hydrazine, dimethyl sulfoxide (DMSO), and urea (*13*).

MXenes have shown promise as electrode materials for Li-ion batteries and Li-ion capacitors (*13*, *14*). For example, when Li^+ ions intercalate into $Ti_3C_2T_x$, a steady-state capacity of ~410 mAh g^{-1} at 1 C is obtained for additive-free flexible electrodes (*13*). Furthermore, theoretical calculations have predicted that Li^+ ions should diffuse rapidly on Ti_3C_2 surfaces, as well as result in high storage capacities (*15*). However, spontaneous intercalation of cations from aqueous solutions has neither been theoretically predicted nor experimentally demonstrated.

Here, we report on the intercalation of Li^+, Na^+, Mg^{2+}, K^+, NH_4^+, and Al^{3+} ions between the 2D $Ti_3C_2T_x$ layers (Fig. 1A). In most cases, the cations intercalated spontaneously. A schematic of the process is shown in Fig. 1B. The intercalation of some ions, notably Al^{3+}, can additionally be promoted electrochemically. We also report on intercalation-induced high capacitances of flexible $Ti_3C_2T_x$ paper electrodes in aqueous electrolytes.

A large number of salts, bases, and acids were explored (table S1). X-ray diffraction (XRD) patterns showed that, after placing the $Ti_3C_2T_x$ in various salt solutions (fig. S1, A to C), there was a downshift in the (0002) peak position. This downshift shows that in all cases, there was an increase in the c-lattice parameter. For example, the c value of $Ti_3C_2T_x$ increased from 20.3 Å to as much as 25.4 Å when placed in potassium hydroxide (KOH) and ammonium hydroxide (NH_4OH) solutions (fig. S1A). In addition to the compounds listed in fig. S1, A to C, other salts intercalated spontaneously when the MXene powders were immersed in sodium carbonate (Na_2CO_3), sodium hydroxide (NaOH), or lithium hydroxide (LiOH) solutions.

Not all salts behaved similarly. In the case of high-pH solutions such as KOH, NH_4OH, NaOH, LiOH, and several others (table S1), the changes in the interplanar spacing were large (fig. S1A). Conversely, close-to-neutral solutions such as Na, K, and Mg sulfates resulted in smaller changes in c (fig. S1B; see also table S1). No shift in the (0002) peak positions was observed when $Ti_3C_2T_x$ was immersed in acetic or sulfuric acid.

To shed light on whether the cations or anions intercalated the $Ti_3C_2T_x$ layers, we tested three sodium salts with differing anion radii. The results (fig. S1C) showed that the c-axis expansions were comparable and independent of anion radii. Furthermore, energy-dispersive x-ray spectroscopy analysis of $Ti_3C_2T_x$ after treatment in the different sulfate salts (fig. S1B) confirmed the presence of the cations; sulfur was not detected (table S2), confirming that it is the cations that intercalate between the $Ti_3C_2T_x$ layers.

Materials with large specific surface area are typically needed to obtain large capacitances in carbon materials for EDLCs. However, at 23 m^2/g, the surface area of multilayer exfoliated $Ti_3C_2T_x$ is low (*13*). It follows that if double-layer capacitance were the only operative mechanism, one would expect the capacitance for this material to be less than that of (for example) activated graphene by a factor of 100 (*16*). However, as noted above, intercalation capacitance can by far exceed double-layer capacitances calculated solely on the basis of a material's surface area (*6*, *17*).

To test this idea, we fabricated multilayer $Ti_3C_2T_x$ electrodes (see supplementary materials for details) and tested them in NaOH-, KOH-, and LiOH-containing electrolytes using a standard three-electrode asymmetrical setup with an Ag/AgCl reference electrode (fig. S2). The resulting cyclic voltammograms (CVs) are shown in Fig. 2A [see fig. S4 for the corresponding electrochemical impedance spectroscopy (EIS) results]. The rectangular-shaped CVs indicate capacitive behavior in these basic solutions. Note that in all experiments, the open circuit potential (OCP) was taken as the starting potential for the CV scans because 0.1 V above this potential, $Ti_3C_2T_x$ oxidation is observed in aqueous electrolytes (see fig. S3).

To study the effect of a cation's valence on the electrochemical performance of multilayer exfoliated $Ti_3C_2T_x$ electrodes, we performed CV scans in 1 M solutions of potassium and aluminum sulfates and nitrates (Fig. 2B and fig. S4B). Clearly, the responses in the K^+- and Al^{3+}-containing solutions were distinctively different, confirming once again that the cations (and not the anions) are intercalating. The CV plots for K_2SO_4 are almost perfectly rectangular. Conversely, the CV data for the more acidic (see table S3) and less conductive $Al_2(SO_4)_3$ electrolyte yield capacitance values that are significantly lower, and the shape of the CV at 10 mV/s and the EIS results show a higher resistance (Fig. 2B and fig. S4B). To ensure that lower electrolyte conductivity did not limit the capacitive performance, we tested $Ti_3C_2T_x$ in 1 M $Al(NO_3)_3$, which has a conductivity similar to that of 1 M K_2SO_4 (table S3). Although the normalized capacitance did not increase appreciably, the CV loops were definitely more rectangular (Fig. 2B), demonstrating the role of electrolyte conductivity.

Further evidence for cation intercalation and its beneficial effect on capacitance comes from the observation that for some electrolytes, time was needed to reach a steady state or maximum capacitance. For strongly basic electrolytes (table S1), such as KOH solutions, the rectangular CV plots were observed almost immediately and the capacitances did not change with time or cycle number. For other electrolytes, however, there was a slow and gradual increase in capacitance with time. For example, for salts such as $MgSO_4$, the CV area increased steadily with time and the maximum capacity was reached only after 48 hours (see figs. S5 and S6). Unlike what is observed for graphite (*18*), there was no irreversible capacitance loss during the first cycle for any of the electrolytes studied.

The performance of the multilayer $Ti_3C_2T_x$ in all tested electrolytes is summarized in Fig. 2C. The specific capacitances were calculated by integrating the discharge portions of the CV plots. The results clearly showed responses that depended on the electrolytes used. Moreover, the calculated capacitances were quite high for a material with such low surface area.

In situ XRD studies of the intercalation process during cycling showed that electrochemical cycling leads to insignificant changes in the c values. For example, when a $Ti_3C_2T_x$ electrode was cycled in a KOH-containing electrolyte, the c values fluctuated within 0.33 Å as the potential was scanned from –1 to –0.2 V (Fig. 3A). Interestingly, a slight shrinkage in c values was observed with increasing voltage. Similar behavior was observed when $Ti_3C_2T_x$ was cycled in NaOAc-containing electrolyte (fig. S7). The simplest explanation for this observation is that the positively charged ions incorporated in $Ti_3C_2T_x$ increase the electrostatic attraction between layers, in a manner analogous to what is observed for

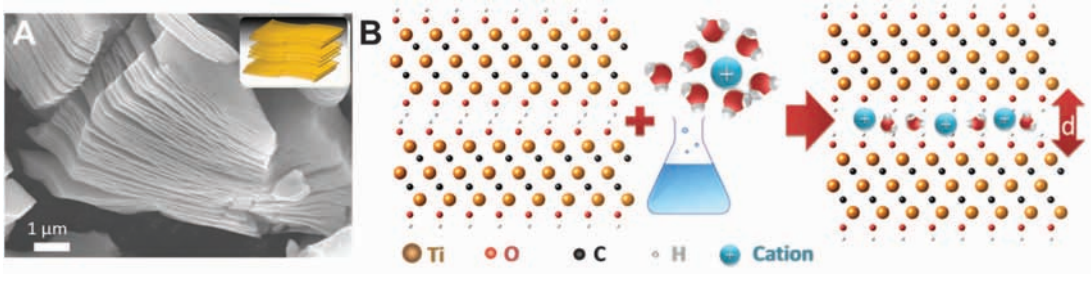

Fig. 1. Intercalation of multilayer exfoliated $Ti_3C_2T_x$. (**A**) Scanning electron micrograph of the $Ti_3C_2T_x$ layered particle. Inset is a schematic of the same, showing the 2D nature of MXenes. (**B**) Schematic illustration of the intercalation of cations between $Ti_3C_2T_x$ layers. The interlayer spacing d increases after ion intercalation.

MnO_2 (*19*). When $Ti_3C_2T_x$ was electrochemically cycled in a $MgSO_4$-containing solution, the shift of the (0002) peak almost doubled relative to the KOH and NaOAc electrolytes (compare Fig. 3A and Fig. 3B). Here again, a slight shrinkage in *c* values was observed with increasing voltage.

To gain further insight into the capacitances and what influences them, we tested MXene "paper" produced by filtering delaminated $Ti_3C_2T_x$ (Fig. 4B). This paper, with a specific surface area of 98 m^2/g, is flexible (inset in Fig. 4B), hydrophilic, additive-free, and conductive. When tested in KOH, the CVs were rectangular, similar to those obtained when multilayer $Ti_3C_2T_x$ powder was used (compare Fig. 4C to Fig. 2A). Furthermore, the EIS results indicated that the $Ti_3C_2T_x$ paper–based capacitors were less resistive (Fig. 4D) than those made with multilayer $Ti_3C_2T_x$ (fig. S4A). This improved electrochemical response can be related to a number of factors, such as the absence of a binder in the system, good contact between the restacked flakes in the paper, increased accessibility of the structure, and thinner electrodes (Fig. 4, A and B).

As shown in Fig. 4E, the use of $Ti_3C_2T_x$ paper electrodes instead of multilayer exfoliated $Ti_3C_2T_x$ in some electrolytes (e.g., KOH and NaOAc) roughly doubled the gravimetric capacitance (see fig. S8 for more information about the performance of $Ti_3C_2T_x$ paper in NaOAc and $MgSO_4$). Even more impressively, the volumetric capacitance values recorded for few-layer $Ti_3C_2T_x$ were on the order of 340 F/cm^3 for KOH (Fig. 4C and fig. S9). Those values are much higher than those found for activated graphene [60 to 100 F/cm^3 (*15*, *20*)] or micrometer-thin carbide-derived carbon electrodes [180 F/cm^3 (*21*, *22*)]. Extreme values for MnO_2 hybrid electrodes [1200 F/cm^3 (*23*); 640 F/cm^3 (*24*)] were obtained on thin films of supported nanoparticles, and therefore cannot be compared with our electrodes. A capacitance retention test performed by galvanostatic cycling at 1 A/g showed almost no degradation in performance after 10,000 cycles (Fig. 4F).

Our results show that a variety of cations of various charges and sizes can readily intercalate, from aqueous solutions, both multilayer exfoliated $Ti_3C_2T_x$ and MXene paper made of few layers of $Ti_3C_2T_x$. The phenomenon depends on pH and the nature of the cations. Extensive investigation of the electrochemical properties of the $Ti_3C_2T_x$ in these aqueous electrolytes showed notable intercalation capacitances. The best performance was observed in basic solutions, such as KOH and NaOH for binder-free $Ti_3C_2T_x$ paper. The latter is highly flexible and yielded volumetric capacitance of up to 350 F/cm^3.

As noted, eight MXenes have been reported to date (*10*) and many more have been theoretically predicted (*25*, *26*). Thus, the volumetric capacitances described above are probably far from the maximum values possible for MXenes in general. The flexibility of $Ti_3C_2T_x$ paper (Fig. 4B) also opens the door for the use of MXenes in flexible and wearable energy storage devices (*27*). The fact that a variety of ions, as different as Na^+ and Al^{3+}, can be accommodated between the MXene layers may also enable MXene use in batteries as well as in metal-ion capacitors (battery-supercapacitor hybrids). Thus, this work opens up exciting possibilities of developing improved intercalation electrodes for batteries, supercapacitors, and hybrid devices using a large variety of ions and/or electrode chemistries.

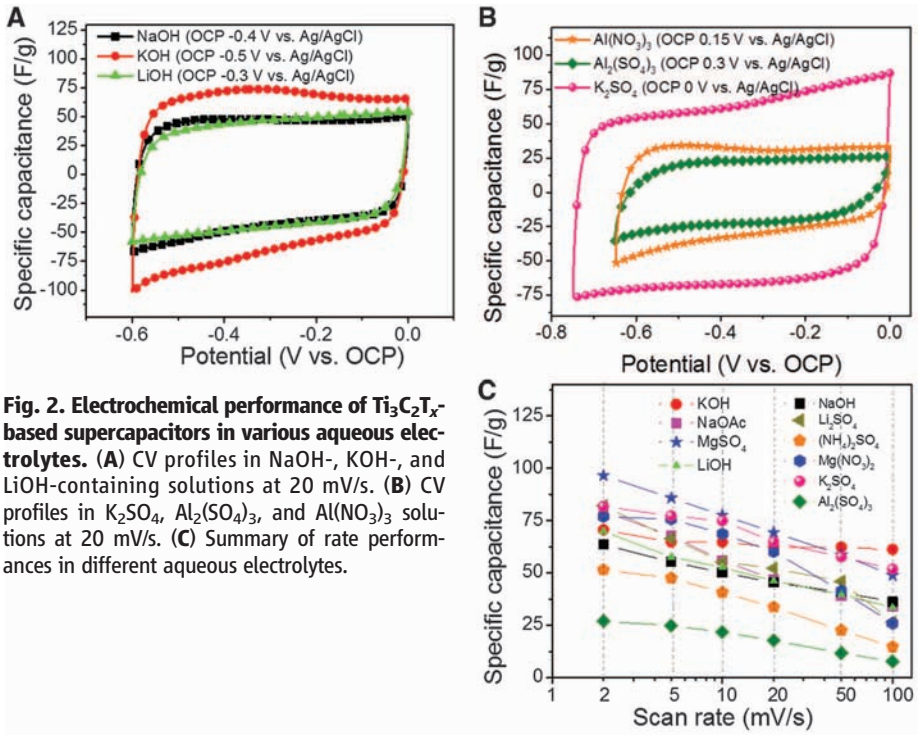

Fig. 2. Electrochemical performance of $Ti_3C_2T_x$-based supercapacitors in various aqueous electrolytes. (**A**) CV profiles in NaOH-, KOH-, and LiOH-containing solutions at 20 mV/s. (**B**) CV profiles in K_2SO_4, $Al_2(SO_4)_3$, and $Al(NO_3)_3$ solutions at 20 mV/s. (**C**) Summary of rate performances in different aqueous electrolytes.

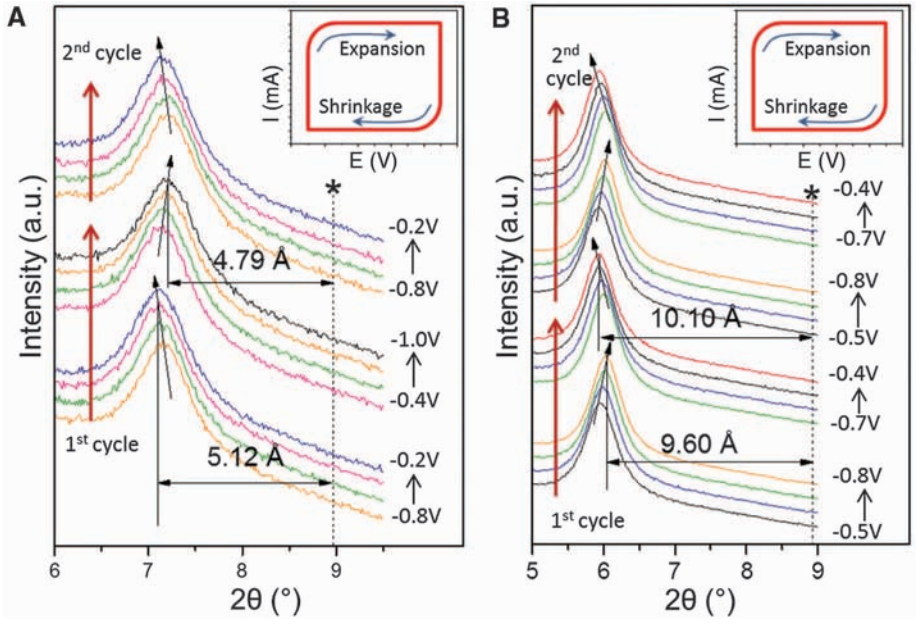

Fig. 3. Electrochemical in situ x-ray diffraction study of multilayer exfoliated $Ti_3C_2T_x$. (**A**) $Ti_3C_2T_x$ in 1 M KOH solution; (**B**) $Ti_3C_2T_x$ in 1 M $MgSO_4$ solution. Vertical dashed lines indicate the original position of the (0002) peak of the $Ti_3C_2T_x$ electrodes before mounting in a cell. Inclined arrows show the direction of the (0002) peak shift. Insets illustrate cycling direction and concomitant changes in *c* lattice parameters during cycling. In both KOH and $MgSO_4$ electrolytes, shrinkage during cathodic polarization is observed.

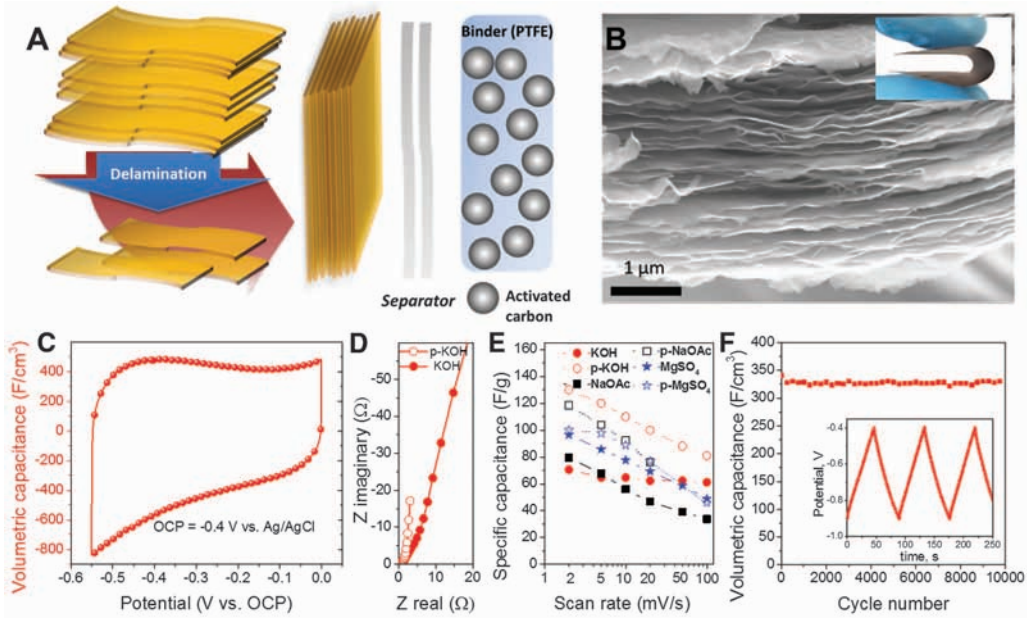

Fig. 4. Electrochemical performance of binder-free $Ti_3C_2T_x$ paper electrodes: (**A**) Schematic of electrode fabrication. During the first stage, the multilayer Ti_3C2T_x powders are delaminated to produce few-layer MXene flakes (see supplementary materials); the resulting colloidal solution is filtered through a porous membrane, producing binder- and additive-free $Ti_3C_2T_x$ paper electrodes for further use in capacitance tests. (**B**) Scanning electron micrograph of paper electrode. Inset is a photograph of the paper showing its flexibility. (**C**) CV of $Ti_3C_2T_x$ paper in KOH electrolyte. (**D**) EIS data in KOH for $Ti_3C_2T_x$ electrode (KOH, solid symbols) and $Ti_3C_2T_x$ paper (p-KOH). (**E**) Rate performance of the $Ti_3C_2T_x$ paper (open symbols) versus multilayer exfoliated $Ti_3C_2T_x$ electrode (solid symbols) in KOH-, $MgSO_4$-, and NaOAc-containing electrolytes. (**F**) Capacitance retention test of $Ti_3C_2T_x$ paper in KOH. Inset: Galvanostatic cycling data collected at 1 A/g.

References and Notes

1. B. Conway, *Electrochemical Supercapacitors: Scientific Fundamentals and Technological Applications* (Kluwer Academic/Plenum, New York, 1999).
2. P. Simon, Y. Gogotsi, *Nat. Mater.* **7**, 845–854 (2008).
3. I. E. Rauda, V. Augustyn, B. Dunn, S. H. Tolbert, *Acc. Chem. Res.* **46**, 1113–1124 (2013).
4. K. Naoi, W. Naoi, S. Aoyagi, J. I. Miyamoto, T. Kamino, *Acc. Chem. Res.* **46**, 1075–1083 (2013).
5. V. Augustyn *et al.*, *Nat. Mater.* **12**, 518–522 (2013).
6. Z. J. Sun *et al.*, *J. Power Sources* **216**, 425–433 (2012).
7. S. Stankovich *et al.*, *Nature* **442**, 282–286 (2006).
8. D. Li, M. B. Müller, S. Gilje, R. B. Kaner, G. G. Wallace, *Nat. Nanotechnol.* **3**, 101–105 (2008).
9. M. W. Barsoum, T. El-Raghy, *Am. Sci.* **89**, 334 (2001).
10. M. Naguib *et al.*, *Adv. Mater.* **23**, 4248–4253 (2011).
11. M. Naguib *et al.*, *ACS Nano* **6**, 1322–1331 (2012).
12. O. Mashtalir, M. Naguib, B. Dyatkin, Y. Gogotsi, M. W. Barsoum, *Mater. Chem. Phys.* **139**, 147–152 (2013).
13. O. Mashtalir *et al.*, *Nature Commun.* **4**, 1716 (2013).
14. J. Come *et al.*, *J. Electrochem. Soc.* **159**, A1368–A1373 (2012).
15. Q. Tang, Z. Zhou, P. W. Shen, *J. Am. Chem. Soc.* **134**, 16909–16916 (2012).
16. Y. Zhu *et al.*, *Science* **332**, 1537–1541 (2011).
17. L. Mai *et al.*, *Sci. Rep.* **3**, 1718 (2013).
18. P. W. Ruch *et al.*, *Carbon* **48**, 1880–1888 (2010).
19. O. Ghodbane, F. Ataherian, N.-L. Wu, F. Favier, *J. Power Sources* **206**, 454–462 (2012).
20. S. Murali *et al.*, *Nano Energy* 10.1016/j.nanoen.2013.01.007 (2013).
21. J. Chmiola, C. Largeot, P.-L. Taberna, P. Simon, Y. Gogotsi, *Science* **328**, 480–483 (2010).
22. M. Heon *et al.*, *Energy Environ. Sci.* **4**, 135 (2011).
23. X. Lang, A. Hirata, T. Fujita, M. Chen, *Nat. Nanotechnol.* **6**, 232–236 (2011).
24. X. Zhao *et al.*, *ACS Nano* **6**, 5404–5412 (2012).
25. M. Kurtoglu, M. Naguib, Y. Gogotsi, M. W. Barsoum, *MRS Commun.* **2**, 133–137 (2012).
26. M. Khazaei *et al.*, *Adv. Funct. Mater.* **23**, 2185–2192 (2012).
27. J. R. Miller, *Science* **335**, 1312–1313 (2012).

Acknowledgments: We thank B. Duployer and J. Come at Paul Sabatier University for help in electrochemical experiments, V. N. Mochalin and M. Beidaghi for helpful discussions, and the Centralized Research Facility of Drexel University for access to XRD and SEM equipment. MXene synthesis was funded by the U.S. Department of Energy, Office of Vehicle Technologies, Batteries for Advanced Transportation Technologies (BATT) Program, under contract DE-AC02-05CH11231, subcontract 6951370. M.R.L. was supported by the U.S. Department of Energy, Energy Storage Systems Research Program, through Sandia National Laboratory. P.S. was supported by the European Research Council (advanced grant ERC-2011-AdG, project 291543–IONACES) and the Chair of Excellence "Embedded multi-functional nanomaterials" from the EADS Foundation. Collaboration between Drexel University and Paul Sabatier University was supported by the Partner University Fund of the Embassy of France.

Supplementary Materials

www.sciencemag.org/content/341/6153/1502/suppl/DC1
Materials and Methods
Supplementary Text
Figs. S1 to S9
Tables S1 to S4
References (*28*, *29*)

10.1126/science.1241488

st